

Direct simulation of liquid-gas-solid flow with a free surface lattice Boltzmann method

Simon Bogner^a, Jens Harting^{a,b} and Ulrich Rüde^c

^a*Forschungszentrum Jülich, Helmholtz-Institut Erlangen-Nürnberg für Erneuerbare Energien, Fürther Straße 248, 90429 Nürnberg, Deutschland;* ^b*Faculteit Technische Natuurkunde, Technische Universiteit Eindhoven, P.O. Box 513, 5600 MB Eindhoven, Nederland;* ^c*Lehrstuhl für Systemsimulation, Universität Erlangen-Nürnberg, Cauerstraße 11, 91058 Erlangen, Deutschland*

(Received 00 Month 20XX; final version received 00 Month 20XX)

Direct numerical simulation of liquid-gas-solid flows is uncommon due to the considerable computational cost. As the grid spacing is determined by the smallest involved length scale, large grid sizes become necessary – in particular if the bubble-particle aspect ratio is on the order of 10 or larger. Hence, it arises the question of both feasibility and reasonability. In this paper, we present a fully parallel, scalable method for direct numerical simulation of bubble-particle interaction at a size ratio of 1-2 orders of magnitude that makes simulations feasible on currently available super-computing resources. With the presented approach, simulations of bubbles in suspension columns consisting of more than 100 000 fully resolved particles become possible. Furthermore, we demonstrate the significance of particle-resolved simulations by comparison to previous unresolved solutions. The results indicate that fully-resolved direct numerical simulation is indeed necessary to predict the flow structure of bubble-particle interaction problems correctly.

Keywords: lattice Boltzmann method; free surface flow; particle suspension simulation; liquid-gas-solid flow; bubble simulation

1. Introduction

Due to the computational complexity of fluid-solid and liquid-gas-solid flow problems, numerical solutions are usually based on homogenized models (Pan et al. 2016; Panneerselvam, Savithri, and Surender 2009; Li and Zhong 2015). Homogenized models do not resolve all involved scales and model the phase interaction based on closure relations (drag correlations) instead. The closure relations, in turn, are obtained from experiments, or – with the advent of high-speed computers – by direct numerical simulation (DNS) of systems of smaller size. DNS techniques allow the most accurate predictions by resolving even the smallest relevant length scales. For fluid-solid, particulate flows the smallest typical length scale is the particle diameter. For the case of fluid-solid flows, new drag correlations have been derived from numerical data (Beetstra, van der Hoef, and Kuipers 2007; Tenneti, Garg, and Subramaniam 2011; Bogner, Mohanty, and Rüde 2014; Tang et al. 2015). Also, DNS has helped to investigate the behavior of particle suspensions and to study hydrodynamic interaction in particulate flows (Aidun and Clausen 2010; Tenneti and Subramaniam 2014) in full detail. Due to computational costs, the system sizes that can be realized by DNS are limited compared to unresolved and homogenized models. Nevertheless, DNS is an important tool that allows the study of flow structures in every detail, and provides the most accurate solutions.

*Corresponding author. Email: s.bogner@fz-juelich.de

To date, only few direct numerical simulation models for liquid-gas-solid flows (LGS) can be found in literature. A numerical method for this class of flows must combine a two-phase flow solver (Scardovelli and Zaleski 1999; Tryggvason, Scardovelli, and Zaleski 2011) with a structural solver for the suspended solid phase. Most LGS simulation approaches (Li, Zhang, and Fan 1999; Chen and Fan 2004; van Sint Annaland, Deen, and Kuipers 2005b; Xu, Liu, and Tang 2013; Sun and Sakai 2015; Li and Zhong 2015) do not fully resolve the particle geometry within the flow. This means that hydrodynamic interaction between particles cannot be captured fully in these models which thus do not count as DNS models according to the narrower definition applied here. Nevertheless, these approaches make use of discrete particle methods (Bićanić 2004; Deen et al. 2007) to resolve particle-particle collisions. The first models to resolve both bubble and particle geometries have been presented by Deen, van Sint Annaland, and Kuipers (2009) and Baltussen et al. (2013). These DNS models combine a front-tracking liquid-gas method with an immersed boundary approach (Mittal and Iaccarino 2005) to couple the flow with the particle simulation. Recently, the same group applied their methodology to study the effective drag on bubbles and particles in liquid flow (Baltussen, Kuipers, and Deen 2017). Presumably due to computational limitations, the simulated systems contain bubbles and particles of similar size only. In many situations of practical relevance, however, the particle size is much smaller than the bubble size. Alternatively, there are efforts to combine diffusive multiphase models with particle models (Stratford et al. 2005; Jansen and Harting 2011; Joshi and Sun 2009). These DNS models work with fully resolved particles, but additional limitations arise from the necessity to resolve also the liquid-gas interface – especially at a high density difference. The density ratio is on the order of $\mathcal{O}(10)$ in these models, which is much smaller than the density ratio of most liquid-gas two-phase flows. Only recently, ? have reached high density ratios for special cases.

In the following, we present a DNS model for liquid-gas-solid flow that allows the simulation of bubble-particle interaction in containing liquid. The model is based on the free surface lattice Boltzmann method (FSLBM) of (Körner et al. 2005) for high liquid-gas density ratios combined with the particulate flow model of (Ladd 1994; Ladd and Verberg 2001). Based on a previous effort (Bogner and Rüde 2013), we have developed a model that is inherently parallel and allows bubble sizes one order of magnitude larger than the particle size while still fully resolving the single particle geometries. Since the grid spacing must be smaller than the particle diameter, the total number of lattice sites is necessarily large and the computational cost is considerable. Therefore, the model is implemented based on a parallel software framework (Feichtinger et al. 2011), that has already been used to realize massively parallel simulations of suspensions (Götz et al. 2010) and bubbly flows (Donath et al. 2009). The new liquid-gas-solid model enables detailed studies of particle transport in the wake of rising bubbles. We demonstrate that our model is capable of predicting important suspension properties, such as increased effective viscosity with solid volume fraction correctly. The terminal rise velocity of a gas bubble decreases accordingly in simulations. Furthermore, we validate the free surface model for different bubble regimes according to the classification of Grace (spherical, ellipsoidal, skirted, dimpled), and present examples of particle transport and mixing in the wake of a single rising bubble for the different regimes. The cost of the DNS is considerable. However, a comparison of the results to previous unresolved simulations indicates the necessity of DNS to predict the full characteristics of the flow and the induced particle transport.

2. Method

In the following, we use a hybrid method based on the free surface lattice Boltzmann method (FSLBM) of Körner et al. (2005) and the particulate flow model of Ladd (1994); Ladd and Verberg (2001). The computational domain is subdivided into the three disjoint regions, corresponding each to the space occupied by liquid, gas, or solid phase, respectively.

2.1. Hydrodynamic Lattice Boltzmann Model

To solve the hydrodynamic equations for the liquid region, we use a D3Q19 lattice Boltzmann model (Wolf-Gladrow 2005; Qian, d’Humières, and Lallemand 1992) on a Cartesian grid. The lattice velocities are denoted by \mathbf{c}_q with $q = 0, \dots, 18$ and have units of grid spacing δ_x per time step δ_t . The data f_q with $q = 0, \dots, 18$ of the scheme is also called *particle distribution function* (PDF). The *lattice Boltzmann equation* of the model can be written as,

$$f_q(\mathbf{x} + \mathbf{c}_q \delta_t, t + \delta_t) = f_q^*(\mathbf{x}, t), \quad (1a)$$

$$f_q^*(\mathbf{x}, t) = f_q(\mathbf{x}, t) + \lambda_- f_q^{\text{neq},-} + \lambda_+ f_q^{\text{neq},+}, \quad (1b)$$

where $f^*(\mathbf{x}, t)$ has been substituted, and is referred to as the *post-collision* state. The upper-indices “+/-” denote the even/odd parts of the respective function. The right hand side of Eq. (1b) corresponds to the two relaxation time collision operator of Ginzburg, Verhaeghe, and d’Humières (2008), with the odd and even eigenvalues $\lambda_-, \lambda_+ \in (-2, 0)$. These eigenvalues thus control the relaxation of the even and odd parts of the non-equilibrium,

$$f_q^{\text{neq}}(\mathbf{x}, t) = f_q(\mathbf{x}, t) - f_q^{\text{eq}}(\mathbf{x}, t), \quad (2)$$

defined as the deviation from the equilibrium function $f_q^{\text{eq}} = e_q(\rho(\mathbf{x}, t), \mathbf{u}(\mathbf{x}, t))$, given as the polynomial

$$e_q(\rho, \mathbf{u}) = \rho w_q \left(1 + \frac{c_{q,\alpha} u_\alpha}{c_s^2} + \frac{u_\alpha u_\beta}{2c_s^4} (c_{q,\alpha} c_{q,\beta} - c_s^2 \delta_{\alpha\beta}) \right), \quad (3)$$

where the w_q , $q = 0, \dots, 18$, are a set of lattice weights, and the constant $c_s = \delta_x / (\sqrt{3} \delta_t)$ is called the *lattice speed of sound*. The *macroscopic* flow variables of pressure and velocity are moments of the PDF, that is,

$$p(\mathbf{x}, t) = c_s^2 \rho(\mathbf{x}, t) = c_s^2 \sum_{q=0}^{18} f_q(\mathbf{x}, t), \quad (4a)$$

$$u_\alpha(\mathbf{x}, t) = \frac{1}{\rho} \sum_{q=0}^{18} c_{q,\alpha} f_q(\mathbf{x}, t). \quad (4b)$$

It can be shown that the velocity field is a second order accurate solution to the incompressible Navier-Stokes equations (Frisch et al. 1987; Holdych et al. 2004; Junk, Klar, and Luo 2005) with kinematic viscosity

$$\nu = - \left(\frac{1}{\lambda_+} + \frac{1}{2} \right) c_s^2 \delta_t. \quad (5)$$

While the first relaxation parameter λ_+ is chosen according to the desired flow viscosity, the second parameter λ_- is fixed to satisfy the equation,

$$\left(\frac{1}{\lambda_+} + \frac{1}{2} \right) \left(\frac{1}{\lambda_-} + \frac{1}{2} \right) = \frac{3}{16}. \quad (6)$$

This “magic” parameterization is optimal for straight axis aligned wall boundaries (Ginzburg and Adler 1994), and yields viscosity independent solutions in general geometries (Ginzburg and d’Humières 2009).

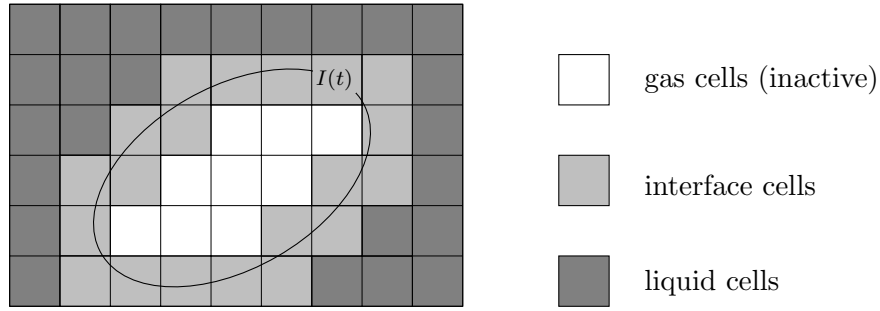


Figure 1.: A fictitious interface $I(t)$ and its discrete FSLBM representation consisting of gas, interface, and liquid nodes.

2.2. Free Surface Lattice Boltzmann Method (FSLBM)

The FSLBM is an interface capturing scheme that is based on the *volume of fluid* (Hirt and Nichols 1981; Tryggvason, Scardovelli, and Zaleski 2011) approach. The *fill level* or *volume fraction* $\varphi(\mathbf{x})$ serves as indicator function. For each node \mathbf{x} , the fill level $\varphi(\mathbf{x})$ is defined as the volume fraction of liquid within the cubic cell volume around \mathbf{x} . Figure 1 shows that three different types of cells can be distinguished:

- $C_g(t)$: the set of *gas nodes*, where $\varphi = 0$.
- $C_l(t)$: the set of *liquid nodes*, where $\varphi = 1$.
- $C_i(t)$: the set of *interface nodes*, where $0 < \varphi \leq 1$. An interface node \mathbf{x} always has a liquid neighbor $\mathbf{x} + \delta_t \mathbf{c}_p \in C_l$ and a gas neighbor $\mathbf{x} + \delta_t \mathbf{c}_q \in C_g$ for some $p, q = 1, \dots, 18$.

The nodes in $C_l \cup C_i$ are active lattice Boltzmann nodes. Introducing further the set of obstacle nodes $C_s(t)$ that are not part of the fluid domain (e.g., walls or nodes that are blocked out by particles), $C_g \cup C_s$ forms the set of inactive nodes within the simulation domain.

The set of interface nodes C_i is exactly the set of boundary nodes that possess a neighbor in the gas subdomain. If an interface node $\mathbf{x}_b \in C_i$ has a gas neighbor $\mathbf{x} + \delta_t \mathbf{c}_q \in C_g$, then the boundary condition of Körner et al. (2005),

$$f_{\bar{q}}(\mathbf{x}_b, t + 1) = -f_q^*(\mathbf{x}_b, t) + 2e_q^+(\rho_w, \mathbf{u}_w), \quad (7)$$

is applied for the opposite direction \bar{q} with $-\mathbf{c}_q = \mathbf{c}_{\bar{q}}$. Here, $p_w = c_s^2 \rho_w$ defines the boundary value for pressure, and \mathbf{u}_w represents the flow velocity at the boundary. It can be shown that Eq. (7) yields a first order approximation of a free boundary (Bogner, Ammer, and Rüde 2015).

The interface capturing scheme is updated according to the flow simulation in every time step. The indicator function $\varphi(\mathbf{x}, t)$ is updated directly from the lattice Boltzmann data.

$$\varphi(\mathbf{x}_i, t + 1) = \varphi(\mathbf{x}_i, t) + \frac{1}{\rho(\mathbf{x}_i, t + 1)} \left(\sum_{q=1}^{Q-1} \Delta m_q(\mathbf{x}_i, t) \right), \quad (8a)$$

with the direction-dependent exchange mass

$$\Delta m_q(\mathbf{x}_i, t) = \begin{cases} 0 & \text{if } \mathbf{x}_i + \mathbf{c}_q \notin (C_i \cup C_l), \\ \frac{1}{2}(\varphi(\mathbf{x}_i + \mathbf{c}_q) + \varphi(\mathbf{x}_i))(f_{\bar{q}}(\mathbf{x}_i + \mathbf{c}_q) - f_q(\mathbf{x}_i)) & \text{if } \mathbf{x}_i + \mathbf{c}_q \in C_i, \\ f_{\bar{q}}(\mathbf{x}_i + \mathbf{c}_q) - f_q(\mathbf{x}_i) & \text{if } \mathbf{x}_i + \mathbf{c}_q \in C_l, \end{cases} \quad (8b)$$

The sets C_l , C_i , and C_g are updated according to the rules illustrated in Fig. 2, where each arrow corresponds to a possible state transition: The transitions between gas, liquid, and interface state, are triggered according to the fill levels φ of the interface cells. Whenever the fill level of an interface cell becomes equal to 0 (equal to 1), then a conversion into a gas cell (liquid cell) is

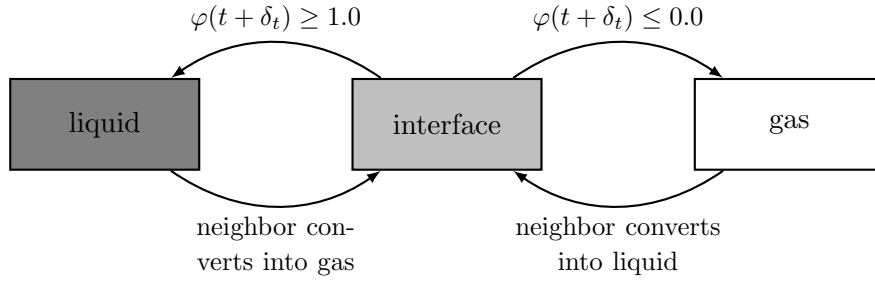


Figure 2.: Possible cell state conversions in FSLBM simulations. Conversions of interface cells are triggered by the fill level φ and, for gas and liquid cells, by conversions of neighboring interface cells into liquid or gas, respectively. (Bogner 2017)

triggered. If needed, inverse transitions from liquid (gas) into interface state are performed in order to close the layer of interface cells. If a gas node changes to interface state, then its LBM data is initialized based on the equilibrium, Eq. (3). Details can be found in Körner et al. (2005) and in (Bogner and Rude 2013) for moving particles.

Since the flow of the gas phase is not simulated in the free surface model, a special treatment of the individual bubbles, i.e., connected regions of gas, is necessary (cf. Anderl et al. 2014; Caboussat 2005; Körner et al. 2005). Such a *bubble model* conserves the mass in the gas phase and provides the local gas pressure p_g needed to define the boundary condition Eq. (7).

For the simulation of capillary flows, the Laplace pressure jump across the interface can be included in Eq. (7). The boundary value for the pressure is then

$$p_w = p_g(\mathbf{x}, t) + 2\sigma\kappa(\mathbf{x}, t), \tag{9}$$

where p_g is the pressure in the gas bubble and κ is the local curvature of the interface. Following Brackbill, Kothe, and Zemach (1992), the curvature can be computed from the fill levels, based on the equations,

$$\mathbf{n} = \nabla\varphi, \tag{10a}$$

$$\kappa(\mathbf{x}) = -(\nabla \cdot \hat{\mathbf{n}}). \tag{10b}$$

To evaluate these expressions, we use an optimized finite difference scheme according to Parker and Youngs (1992). At the solid particles, perfect wettability is assumed. Further details and alternative curvature computation schemes can be found in Bogner, Rude, and Harting (2016).

2.3. Particulate Flow Simulation

Each (spherical) particle is defined by its radius R_P , specific density ρ_P , and a Lagrangian description consisting of position $\mathbf{x}_P(t)$, velocity $\mathbf{u}_P(t)$, and angular velocity $\omega_P(t)$. Any grid node inside of a particle is called obstacle node. Whenever a liquid node \mathbf{x}_b is next to an obstacle node covered by particle P , then the *bounce-back* rule with velocity term,

$$f_{\bar{q}}(\mathbf{x}_b, t + 1) = f_{\bar{q}}^*(\mathbf{x}_b, t) - 2e_{\bar{q}}^-(\rho_w, \mathbf{u}_w), \tag{11}$$

is used to impose the particle surface velocity,

$$\mathbf{u}_w = \mathbf{u}_P + \omega_P \times (\mathbf{x}_w - \mathbf{x}_P), \tag{12}$$

at the boundary. In Eq. (11), ρ_w is substituted with the density value of the boundary point from the previous time step.

For the time integration of the particle data, the hydrodynamic force \mathbf{F}_P and torque \mathbf{T}_P are computed from the lattice Boltzmann data. Based on the *momentum exchange principle*, one computes

$$\mathbf{F}_P = \sum_{\mathbf{x} \in B_P} \sum_{q \in I_P(\mathbf{x})} \Delta \mathbf{j}_q(\mathbf{x}) \frac{\delta_x^3}{\delta_t}, \quad (13)$$

$$\mathbf{T}_P = \sum_{\mathbf{x} \in B_P} \sum_{q \in I_P(\mathbf{x})} (\mathbf{x} - \mathbf{x}_P) \times \Delta \mathbf{j}_q(\mathbf{x}) \frac{\delta_x^3}{\delta_t}, \quad (14)$$

where

$$\Delta \mathbf{j}_q(\mathbf{x}) := \mathbf{c}_q f^*(\mathbf{x}, t) - \mathbf{c}_q f(\mathbf{x}, t + 1), \quad (15)$$

is used to approximate the momentum transferred along a single boundary-intersecting link at a boundary node \mathbf{x} (Ladd 1994; Ladd and Verberg 2001). In Eqs. (13) and (14), the set B_P is the set of all nodes surrounding the particle P with a nonempty set $I_P(\mathbf{x}_b)$ of particle surface intersecting links. If B_P contains lattice nodes on the inside of another particle, the equilibrium distribution is assumed in Eq. (15).

The hydrodynamic lubrication forces obtained by Eq. (13) are valid only if the gap between two particles P_1, P_2 is sufficiently resolved. Hence, if the gap size becomes smaller than $\Delta_c = 2/3\delta_x$, then a *lubrication correction*,

$$\mathbf{F}_{P_1, P_2}^{lub} = -\frac{6\pi\mu(R_{P_1}R_{P_2})^2}{(R_{P_1} + R_{P_2})^2} \left(\frac{1}{|\mathbf{x}_{1,2}| - R_{P_1} - R_{P_2}} - \frac{1}{\Delta_c} \right) \hat{\mathbf{x}}_{1,2} \cdot (\mathbf{u}_{P_1} - \mathbf{u}_{P_2}) \hat{\mathbf{x}}_{1,2}, \quad (16)$$

is added to the net force \mathbf{F}_{P_1} , where $\mathbf{x}_{1,2} = \mathbf{x}_{P_2} - \mathbf{x}_{P_1}$ is the relative position of the particles (Ladd and Verberg 2001). Here, $\mu = \rho\nu$ is the dynamic viscosity. This improves the simulation of hydrodynamic interaction between particles (Aidun and Clausen 2010). Since Eq. (16) diverges for $|\mathbf{x}_{1,2}| \rightarrow 0$, the gap size is limited from below to be at least $0.2\Delta_c$. Furthermore, to increase stability at higher solid volume fractions, the time integration of the particles proceeds in up to 10 time steps per LBM step.

The inclusion of wetting boundaries is described in Brackbill, Kothe, and Zemach (1992); Bogner, Rude, and Harting (2016). However, we only study fully wetting particles in the following.

3. Validation of the Numerical Model

The simulations of bubbles in moderately dense suspensions and bubble-particle interaction are found in Sec. 4. Here, we first validate the correct behavior of solid-liquid suspension simulations (Sec. 3.1) and gas-liquid simulations (Sec. 3.2) with our model.

3.1. Validation of Particle Suspension Model

It has been demonstrated in the past that the LBM is valid in the simulation of particle suspensions, e.g., Aidun and Clausen (2010); Ladd and Verberg (2001); Harting et al. (2014); Kromkamp et al. (2006). Here, we reproduce as validation experiment the relative shear viscosity of a spherical particle suspension in a shear flow between plates. Similar to Kromkamp et al. (2006), a domain is initialized with a random particle bed of N spherical particles of radius $R_P = 8\delta_x$ and specific

density $\rho_s = 8$. The domain size is fixed to $V = 114\delta_x \times 116\delta_x \times 180\delta_x$, altering N to realize different solid volume fractions

$$\Phi = \frac{NV_P}{V}, \quad (17)$$

where V_P is the particle volume. The flow is initially at rest, and driven by imposing a constant velocity $u_x = \pm 0.01\delta_x/\delta_t$ on the boundary planes at $z = 0$ and $z = 180$ in opposed directions, while applying periodicity along x and y directions. The effective viscosity μ_s of the numerical suspension model is evaluated by measuring the net force \bar{F}_x on the boundary walls,

$$\mu_s = \frac{\bar{F}_x}{A\dot{\gamma}}, \quad (18)$$

where $\dot{\gamma}$ is the shear rate. The resulting force values oscillate due to non-trivial interaction between particles, and must be averaged over a number of time steps T (typically $\dot{\gamma}T \geq 100$). The (particle) Reynolds number is defined as

$$\text{Re}_P = \frac{\rho_f \dot{\gamma} (2R_P)^2}{\mu}, \quad (19)$$

where ρ_f is the fluid density. In [Bogner \(2017\)](#), the same setup was repeated with various solid volume fractions and Reynolds numbers. As shown in [Fig. 3](#), the model correctly predicts the expected increase of effective viscosity with increased solid volume fraction and Reynolds number. [Figure 3a](#) also displays the empirical correlation of Eilers ([Stickel and Powell 2005](#)),

$$\frac{\mu_s(\Phi)}{\mu} = \left[1 + \frac{1.25\Phi}{1 - \Phi/\Phi_{\max}} \right]^2, \quad (20)$$

where $\Phi_{\max} = 0.63$ is assumed as the maximal packing fraction for random sphere packings.

3.2. Validation of Free Surface Model

The FSLBM described in [Sec. 2.2](#) has been validated for the case of single rising bubbles in liquid columns in [Bogner \(2017\)](#), from which the following results are adopted. The behavior of single rising bubbles in a quiescent (infinite) liquid is characterized by three dimensionless numbers ([Clift, Grace, and Weber 1978](#); [Fan and Tsuchiya 1990](#)). The *Morton number* is defined as

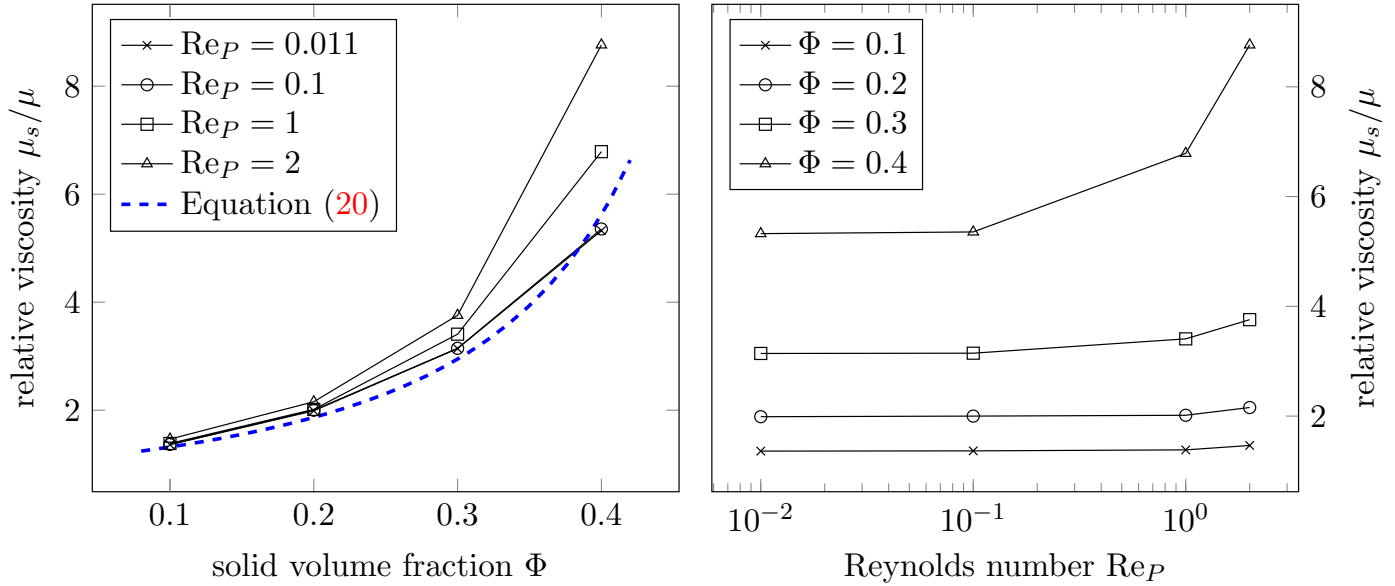
$$\text{Mo} = \frac{g\mu^4\Delta\rho}{\rho^2\sigma^3}, \quad (21)$$

where g is the gravitational constant, μ and ρ are the viscosity and density of the surrounding liquid, and $\Delta\rho$ is the density difference of gas and liquid. The *Eötvös number*,

$$\text{Eo} = \frac{\Delta\rho g d^2}{\sigma}, \quad (22)$$

where d is the diameter of the bubble, characterizes the ratio of buoyancy and surface tension forces. Finally, the bubble Reynolds number is defined as

$$\text{Re}_b = \frac{\rho u_\infty d}{\mu}, \quad (23)$$



(a) Relative viscosity at various solid volume fractions.

(b) Relative viscosity at various Reynolds numbers.

Figure 3.: Simulation of a thickening particle suspension in shear flow. The relative viscosity of the simulated suspension increases with solid volume fraction and Reynolds number. (Bogner 2017)

where u_∞ is the terminal rise velocity of the bubble. The bubble diameter d is understood as the diameter of a volume-equivalent spherical bubble, unless otherwise noted. Based on Grace (1973), the behavior of gas bubbles rising in a liquid column can be classified and allows a prediction of the bubble shape, e.g., spherical, ellipsoidal, spherical cap, skirted, dimpled, etc., or can be used to estimate the terminal rise velocity u_∞ of the bubble, if Eo and Mo are given. Alternatively, one can work with the correlation of Fan and Tsuchiya (1990),

$$\tilde{u}_\infty = \left[\left(\frac{Mo^{-1/4} Eo}{K_b} \right)^{-n} + \left(\frac{2c}{\sqrt{Eo}} + \frac{\sqrt{Eo}}{2} \right)^{-n/2} \right]^{1/n}, \quad (24)$$

where \tilde{u}_∞ is the nondimensional rise velocity. Velocity and diameter are made nondimensional using

$$\tilde{u} = u \left(\frac{\rho}{\sigma g} \right)^{1/4}, \quad \text{and} \quad \tilde{d} = d \left(\frac{\rho g}{\sigma} \right)^{1/2}. \quad (25)$$

In Eq. (24), the parameters K_b , c , and n , are chosen to account for special material properties not covered by Re , Mo , and Eo . The parameter n ranges from 0.8 to 1.6 depending on the liquid purity, while c is chosen as 1.2 (single-component liquid) or 1.4 (multi-component liquid). The value of K_b is adapted as

$$K_b = \max(12, K_{b0} Mo^{-0.038}), \quad (26)$$

where K_{b0} depends on the liquid (e.g., $K_{b0} = 14.7$ for water). Like the Grace diagram, correlation Eq. (24) is obtained from experimental data, and can predict u_∞ with an error of about $\pm 10\%$.

Van Sint Annaland, Deen, and Kuipers (2005a) suggest four different bubble regimes for the validation of a two-phase volume of fluid solver, that are used as a reference in the following. The Mo and Eo numbers used in the following simulations (Table 1) have been chosen to represent the

case	μ [Pa s]	σ [$\frac{N}{m}$]	g [$\frac{m}{s^2}$]	Mo	Eo	Re_b	Re_b^*
A (spherical)	0.25	0.145	0.981	1.26×10^{-3}	0.974	1.66	1.76
B (ellipsoidal)	0.42	0.145	9.81	0.100	9.74	4.18	4.43
C (skirted)	0.13211	0.014545	9.81	0.9711	97.1	18.56	14.53
D (dimpled)	0.75	0.014545	9.81	1018	97.4	1.58	1.46

Table 1.: Test cases for different bubble regimes. Re_b is the expected Reynolds number for infinite domains according to Eq. (24) with $n = 1.0$, $c = 1.2$ and $K_{b0} = 14$ in Eq. (26). Re_b^* is the value obtained in FSLBM simulations in a finite domain with free-slip walls. Simulations were parameterized according to the given viscosity μ , liquid-gas surface tension σ , and gravitational constant g , assuming a liquid mass density of $\rho = 1000kg/m^3$.

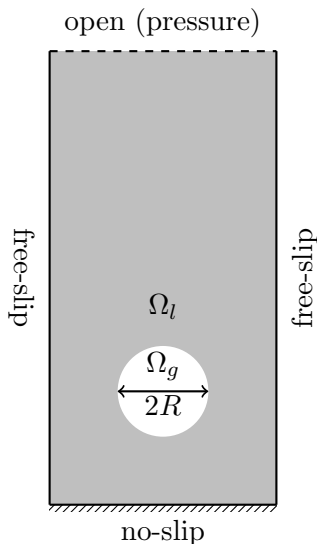


Figure 4.: Boundary conditions around liquid column for rising bubble simulations. At $t = 0$, a spherical bubble Ω_g of diameter $2R$ is initialized, surrounded by quiescent liquid Ω_l .

test cases suggested by [van Sint Annaland, Deen, and Kuipers \(2005a\)](#). In this reference, the surface tension modeling is based on [Brackbill, Kothe, and Zemach \(1992\)](#), similar to our finite difference model. The authors suggest free-slip boundary conditions for all lateral directions, no-slip at the bottom, and a pressure boundary at the top of the domain. A sketch of the domain and initial conditions is shown in Fig. 4. The fluid parameters for the simulation collected in Tab. 1 are given with respect to a liquid of density $\rho = 1000kg/m^3$. The grid spacing is $\delta_x = 10^{-3}m$ and the time step is $\delta_t = 10^{-4}s$. As a compromise between computational cost and influence of the finite domain size on the bubble dynamics, a domain size of $40 \times 40 \times 100$ nodes is recommended by the authors. Here, we directly adopt the resolution and the domain size of the original. The initial condition consists of a *spherical* bubble of $R = 6\delta_x$ centered around the position $(20, 20, 10)\delta_x$ in a column of quiescent liquid.

For $t \geq 0$, the initially spherical bubble starts to accelerate due to the pressure gradient until it reaches a terminal velocity and the bubble shape does not change any more. Figure 5 shows the simulated bubble shapes using a triangulation of the smoothed indicator function contour surface $\varphi = 0.5$. For each case, the simulated bubble shape agrees well with the predictions according to the Grace diagram. The velocity field around the bubble is shown in Fig. 6. As reported also by [van Sint Annaland, Deen, and Kuipers \(2005a\)](#), the terminal velocities obtained from simulations agree reasonably well with the predictions of experimental relations. Table 1 lists the simulated terminal Reynolds number Re_b^* in comparison to the prediction according to Eq. (24).

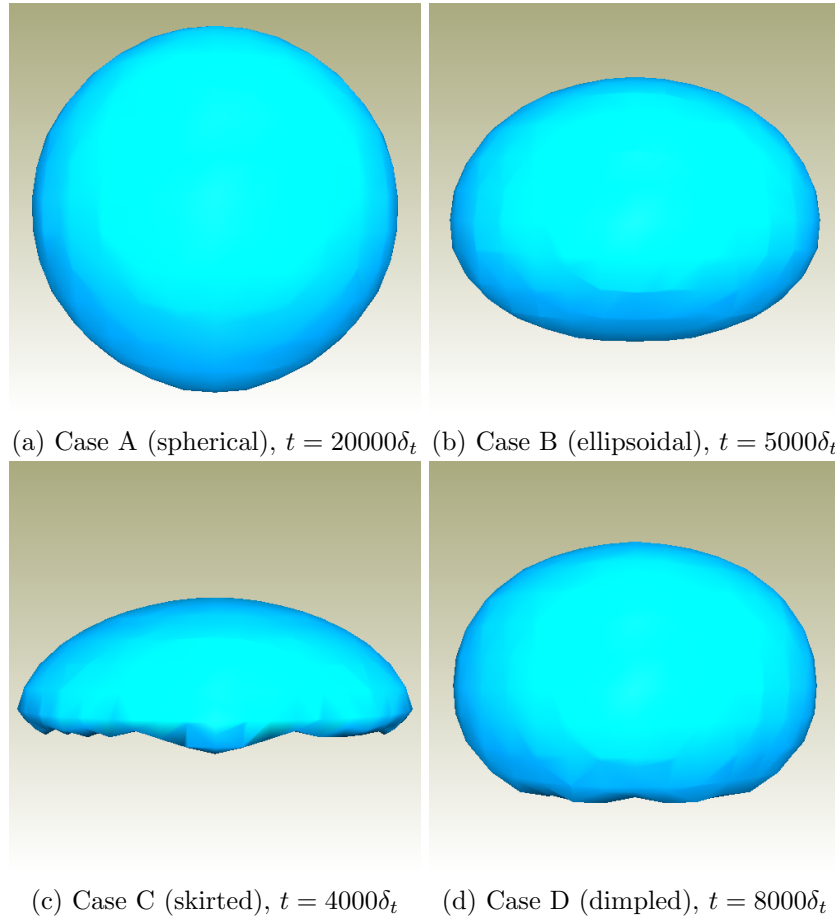


Figure 5.: Bubble shapes obtained from simulations of the bubble regimes from Tab. 1.

4. Results

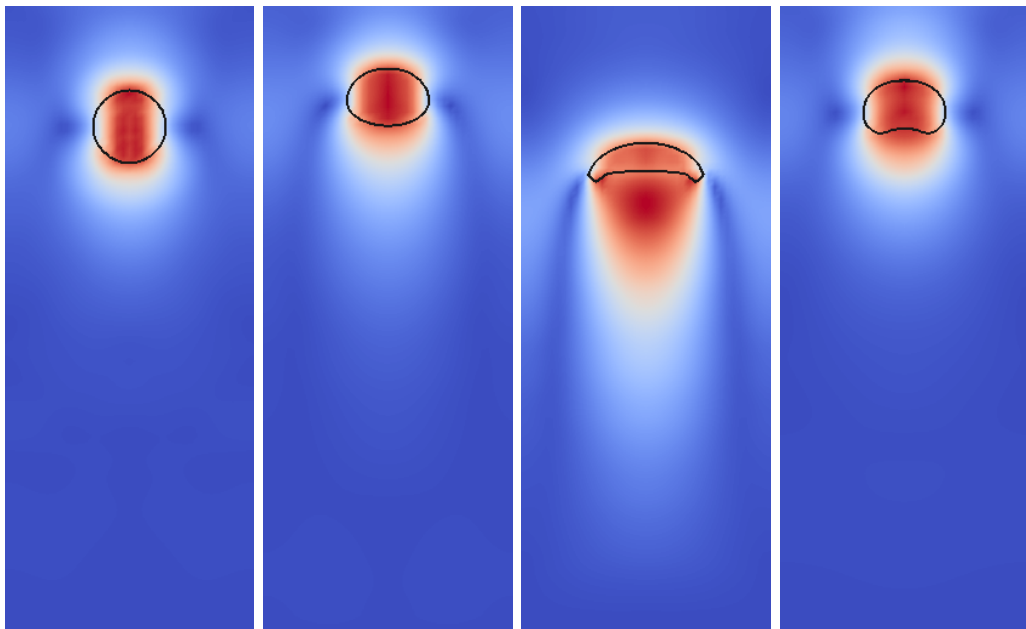
4.1. Bubble Particle Interaction

We now study cases of bubble-particle interaction. Again, the basic setup consists of a liquid column containing a single bubble of radius $R = 0.01m$ rising within a bed of spherical particles of radius $R_P = 8 \cdot 10^{-4}m$. Using a grid spacing of $\delta_x = 8 \cdot 10^{-5}m$, the size of the computational domain is $500 \times 500 \times 1300$ lattice cells surrounding the initially spherical bubble at $(250, 250, 250)\delta_x$. This means that each particle is resolved by 5 lattice cells per diameter. The surface tension σ is $0.145N/m$ and the gravity is assumed to be $0.981m/s^2$, such that the spherical bubble regime is expected, in a fluid of density is $\rho = 1000kg/m^3$ and viscosity $\mu = 0.25kg/(ms)$. Within the liquid column, a homogeneous particle bed is initialized by choosing random positions. The bed density Φ varies with the particle number N ,

$$\Phi = \frac{NV_P}{V - V_b}, \quad (27)$$

where $V_P = 4/3\pi R_P^3$ is the particle volume and $V_b = 4/3\pi R^3$ is the bubble volume. The solid mass density is $\rho_s = 3000kg/m^3$. At the given bubble-particle size ratio, the liquid-solid system surrounding the bubble can be viewed as a homogeneous medium of increased density and viscosity. Notice, that the effective time scale of particle sedimentation is low compared to the expected rise velocity of the bubble.

In a series of simulations the bubble is released within the particle bed, and the terminal rise



(a) Case A (spherical), $t = 20000\delta_t$ (b) Case B (ellipsoidal), $t = 5000\delta_t$ (c) Case C (skirted), $t = 4000\delta_t$ (d) Case D (dimpled), $t = 8000\delta_t$

Figure 6.: Velocity field in the slice $y = 20\delta_x$ of the simulations of the bubbles regimes from Tab. 1. Red color indicates high flow velocity, blue indicates low velocity magnitude. Black lines indicate the free surface.

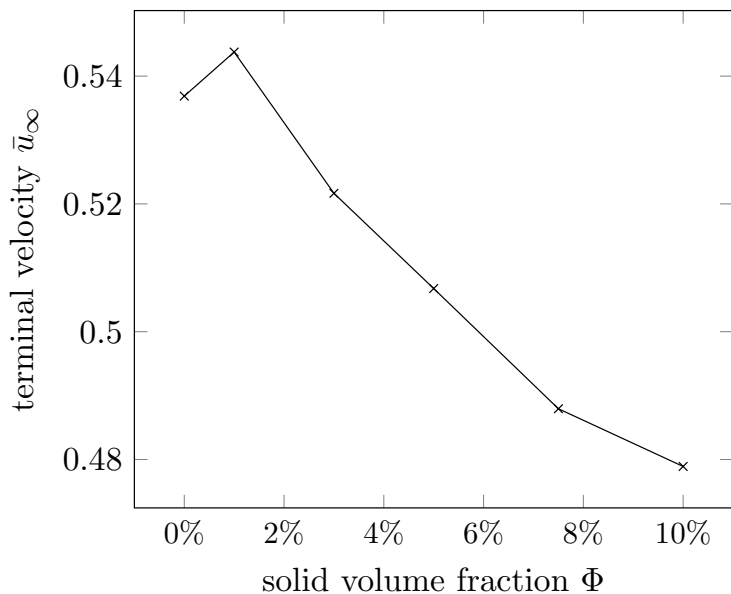
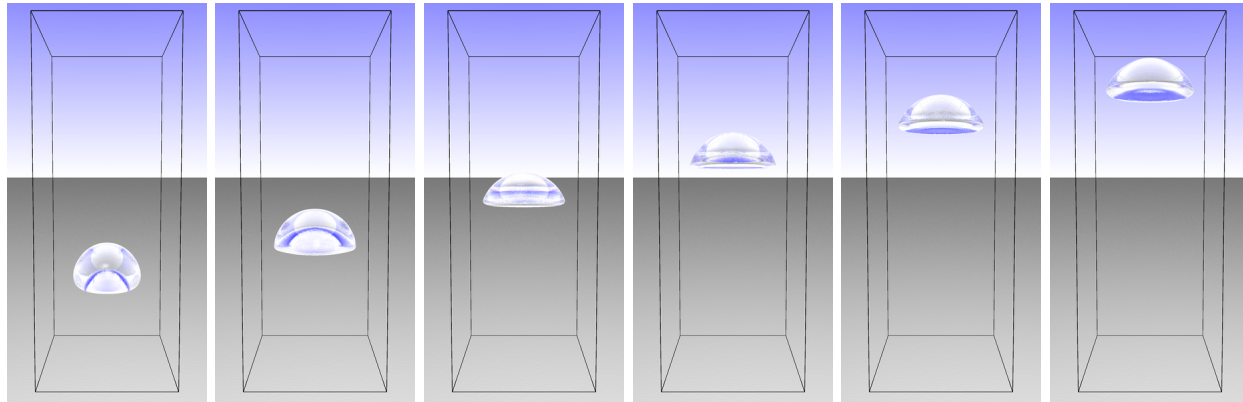
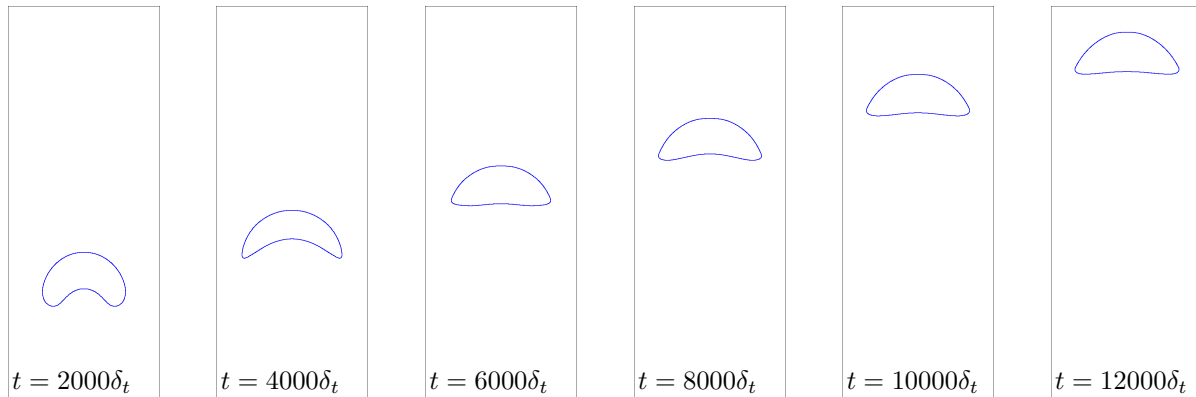


Figure 7.: Dimensionless terminal rise velocity at solid volume fractions from 0 to 10%.

velocity depending on the bed solid volume fraction is evaluated. Figure 7 shows the decrease of bubble velocity with increased bed density. Due to the presence of the particles, the average mass density of the particle suspension around the bubble increases, and the buoyancy force on the bubble is increased. This explains the small increase in velocity from 0 to 1% solid volume fraction. More significantly, with higher solid volume fraction, the higher effective viscosity of the suspension reduces the terminal velocity reached. This is in agreement with experiments from literature, that reports a decreasing rise velocity with increased suspension thickness (Tsuchiya et al. 1997).



(a) Three-dimensional view of the bubble shape within liquid column.



(b) Slice through the center of the domain ($y = 250\delta_x$).

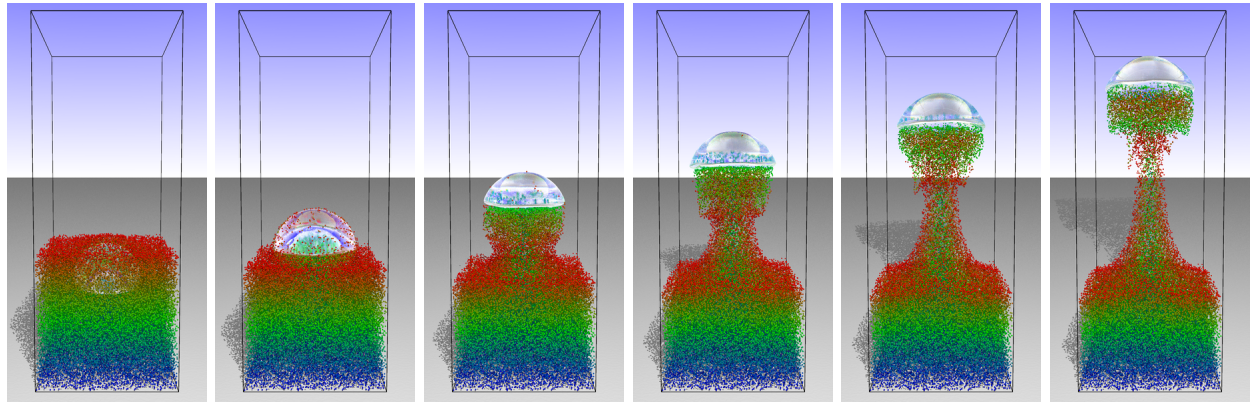
Figure 8.: Bubble rise without particles, at selected time steps (ordered from left to right). The spherical cap shape agrees well with the prediction according to [Grace \(1973\)](#).

We remark that the model is currently limited to low solid volume fractions. For the spatial resolution applied in this work, solid volume fractions of 20% often developed instabilities and nonphysical behavior. The reason seems to be the distribution of particles next to the liquid-gas interface that can make the free-surface algorithm ineffective by covering the cells containing the liquid-gas interface. This is currently a limitation of the model, which might be improved by altering the surface tension model to satisfy the perfect wettability of particles more accurately.

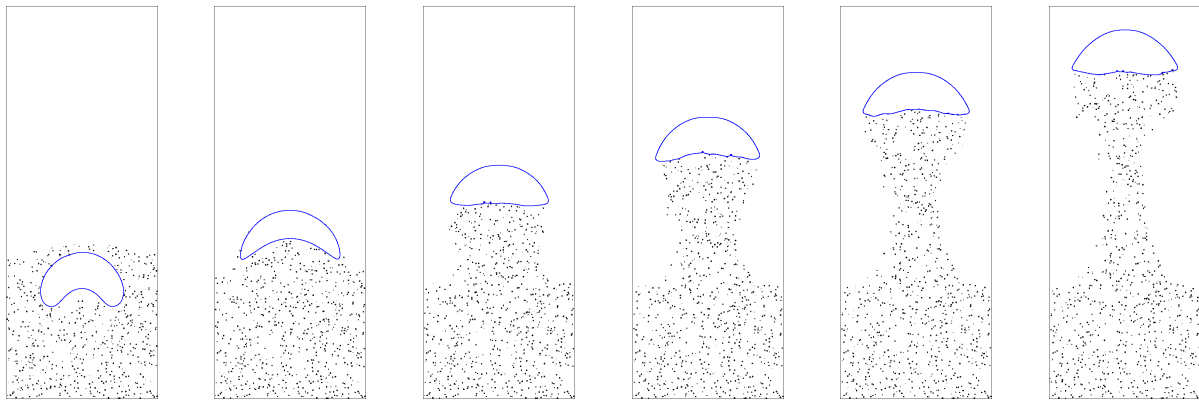
4.2. Simulation of Bubble-Induced Particle Mixing

The particle bed is now limited to the range $z = [0, 500]\delta_x$ that includes the initially spherical bubble. We assume a liquid density of $\rho = 1000\text{kg}/\text{m}^3$, viscosity $\mu = 10^{-1}\text{kg}/(\text{m} \cdot \text{s})$, liquid-gas surface tension $\sigma = 0.1\text{N}/\text{m}$, and a gravity $g = -9.81\text{m}/\text{s}^2$ along the z -axis. Choosing the time step as $\delta_t = 2.5 \cdot 10^{-5}\text{s}$, the lattice relaxation time becomes $\tau \approx 1.672$. The dimensionless numbers for the bubble are $\text{Mo} = 9.81 \cdot 10^{-4}$ and $\text{Eo} = 39.24$, with an expected terminal Reynolds number $\text{Re}_b = 61.73$ according to Eq. (24) (with $n = 1, c = 1.2$). This setup has been chosen similar to a test case of [Deen, van Sint Annaland, and Kuipers \(2007\)](#).

Without any particles ($\Phi = 0$), the terminal rise Reynolds number obtained from simulations is $\text{Re}_b^* = 48$. Again, the lower velocity can be attributed to wall effects. Figures 8 to 10 show the process without particles and at bed densities $\Phi = 2.5\%$ and $\Phi = 10\%$. The terminal rise velocity is hardly affected by the presence of the particles in this case, after the top of the bubble is uncovered from particles. In these images, the particle color indicates the initial z -position of the particle, to show the mixing of different bed layers in the wake of the bubble. A circulating



(a) Three-dimensional view of bubbles and particles. Particle color indicates initial z coordinate of particle position at $t = 0$.



(b) Slice through the center of the domain ($y = 250\delta_x$).

Figure 9.: Bubble rise from a bed consisting of 44 621 particles ($\Phi = 2.5\%$) at selected time steps (times chosen identical to Fig. 8).

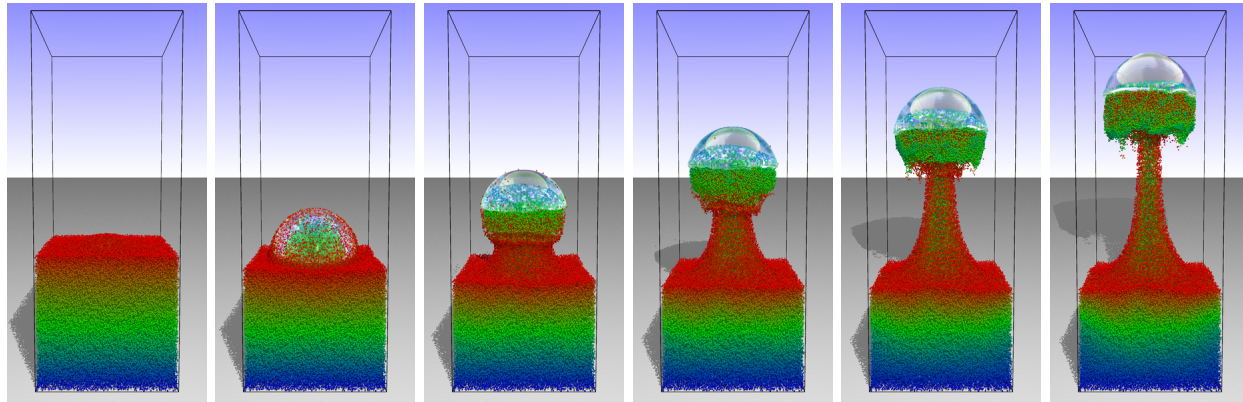
motion is observable in the wake of the bubble. This effect seems to be absent in the unresolved simulations of [Deen, van Sint Annaland, and Kuipers \(2007\)](#), where the recirculation region seems to have no influence on the particles. Also a large number of particles from the middle and lower layer of the bed are carried in the wake of the bubble. That is, we can observe substantial changes in the relative positions of particles during the mixing process.

Figure 11 shows the same setup with altered fluid properties corresponding to different bubble regimes. The wake and particle structure differs significantly in the different regimes. The bubble wake is strongest for the skirted regime that generates the largest recirculation region that also displays the highest solid mass transport. At the other extreme, we find that the spherical case has the least mixing effect and generates only a thin cone of lifted particles.

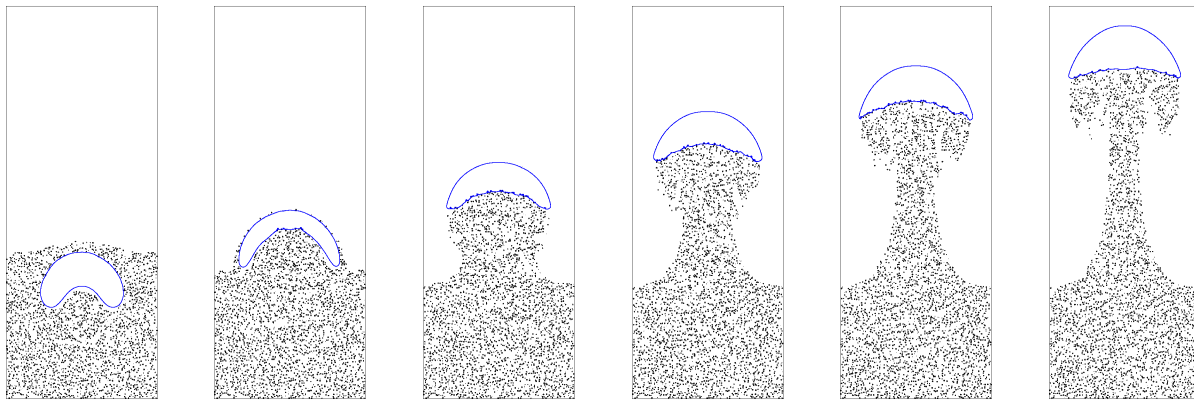
Scenarios of this complexity require a considerable amount of computational cost. The run time in each of the above cases is approximately 6.66 hours when utilizing 2 000 cpu cores of a distributed system in parallel. The considerable complexity stems from the high resolutions required by the DNS. Here, we have used $3.25 \cdot 10^8$ grid points, whereas the unresolved simulations of [Deen, van Sint Annaland, and Kuipers \(2007\)](#) require only $1.6 \cdot 10^5$ grid points.

5. Conclusion

Direct numerical simulation of liquid-gas-solid flows offers the possibility of detailed studies of bubble-particle interaction in liquids. The parallel model proposed in this paper allows, to the



(a) Three-dimensional view of bubbles and particles. Particle color indicates initial z coordinate of particle position at $t = 0$.



(b) Slice through the center of the domain ($y = 250\delta_x$).

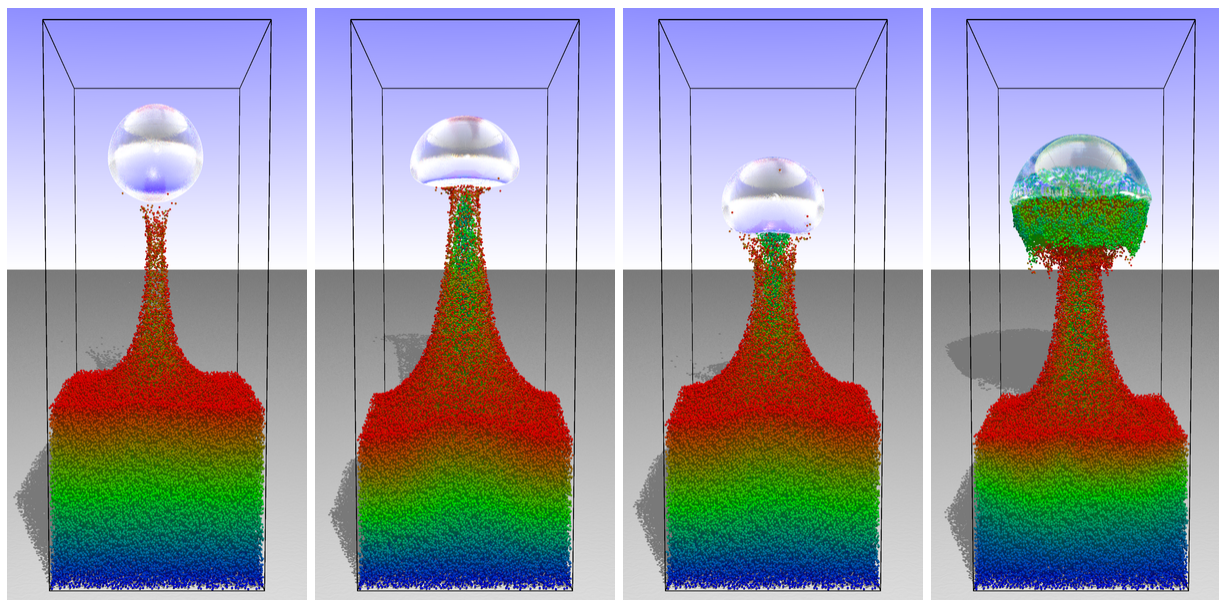
Figure 10.: Bubble rise from a bed consisting of 178 486 particles ($\Phi = 10\%$) at selected time steps (times chosen identical to Fig. 8).

best of our knowledge, for the first time particle-resolved simulations of gas bubbles within slurry columns. This is possible thanks to the parallel design of the model that allows the exploitation of the parallelism of modern supercomputers. It has been demonstrated that the model can simulate particle mixing in the wake of rising gas bubbles. The structures formed by particles in the wake of the bubbles can be studied in great detail. The effect of different bubble regimes, i.e., bubble size and surface tension, on the particle transport can be analyzed. A comparison with previous, unresolved simulations indicates that particle-resolved DNS is indeed necessary to predict this flow structure correctly.

Future research may include particle wettability and structures at liquid-gas interfaces. Also, systematic studies of bubble-particle interactions could be used in improving existing drag correlations for bubbles in particle solutions.

References

- Aidun, C. K., and J. R. Clausen. 2010. “Lattice-Boltzmann Method for Complex Flows.” *Annual Review of Fluid Mechanics* 42: 439–472.
- Anderl, D., S. Bogner, C. Rauh, U. Rde, and A. Delgado. 2014. “Free surface lattice Boltzmann with enhanced bubble model.” *Computers and Mathematics with Applications* 67 (2): 331–339. <http://arxiv.org/abs/1604.01632>.
- Baltussen, M.W., L.J.H. Seelen, J.A.M. Kuipers, and N.G. Deen. 2013. “Direct Numerical Simulations of gasliquid-solid three phase flows.” *Chemical Engineering Science* 100: 293 – 299.



(a) spherical, $E_o = 2.71$, (b) ellipsoidal, $E_o = 27.1$, (c) dimpled, $E_o = 271$, (d) skirted, $E_o = 39.2$,
 $Mo = 1.26 \times 10^{-3}$ $Mo = 9.09 \times 10^{-2}$ $Mo = 1.02 \times 10^3$ $Mo = 9.81 \times 10^{-4}$

Figure 11.: Particles mixing in the wake of bubbles at different bubble regimes (initial bed density $\Phi = 10\%$). The simulations allow a detailed investigation of the wake structure and the accompanying mixing process of the particles. In the spherical case (a), only a thin filament of particles follows the upward motion of the bubble. Hardly any particles from lower layers (green or blue) of the bed are carried upwards. In the ellipsoidal case (b), the effect is stronger and one observes a significant portion of green particles following the bubble wake. Cases (c) and (d) feature a circulating flow in the wake of the bubble. This recirculating region in the wake of the bubble can carry a larger number of particles. The effect is strongest in case (d), where particles from lower layers of the bed (green) change relative position with particles from the top (red).

- Baltussen, M. W., J. A. M. Kuipers, and N. G. Deen. 2017. “Direct numerical simulation of effective drag in dense gas-liquid-solid three-phase flows.” *Chemical Engineering Science* 158: 561.
- Beetstra, R., M. A. van der Hoef, and J. A. M. Kuipers. 2007. “Drag Force of Intermediate Reynolds Number Flow Past Mono- and Bidisperse Arrays of Spheres.” *Fluid Mechanics and Transport Phenomena* 53 (2): 489–501.
- Bićanić, N. 2004. “Discrete Element Methods.” In *Encyclopedia of Computational Mechanics*, John Wiley & Sons, Ltd.
- Bogner, S. 2017. “Direct Numerical Simulation of Liquid-Gas-Solid Flows Based on the Lattice Boltzmann Method.” Ph.D. thesis. University of Erlangen-Nuremberg.
- Bogner, S., R. Ammer, and U. Rüde. 2015. “Boundary Conditions for Free Interfaces with the Lattice Boltzmann Method.” *Journal of Computational Physics* <http://arxiv.org/abs/1409.5645>.
- Bogner, S., S. Mohanty, and U. Rüde. 2014. “Drag correlation for dilute and moderately dense fluid-particle systems using the lattice Boltzmann method.” *International Journal of Multiphase Flow* 68: 71–79. <http://arxiv.org/abs/1401.2025>.
- Bogner, S., and U. Rüde. 2013. “Simulation of floating bodies with the lattice Boltzmann method.” *Computers and Mathematics with Applications* 65: 901–913. <http://arxiv.org/abs/1201.0351>.
- Bogner, S., U. Rüde, and J. Harting. 2016. “Curvature estimation from a volume of fluid indicator function for the simulation of surface tension and wetting with a free surface lattice Boltzmann method.” *Physical Review E* 93 (4): 043302. <http://arxiv.org/abs/1509.07691>.
- Brackbill, J. U., D. B. Kothe, and C. Zemach. 1992. “A Continuum Method for Modeling Surface Tension.” *Journal of Computational Physics* 100: 335–354.
- Caboussat, A. 2005. “Numerical Simulation of Two-Phase Free Surface Flows.” *Archives of Computational Methods in Engineering* 12 (2): 165–224.
- Chen, C., and L.-S. Fan. 2004. “Discrete simulation of gas-liquid bubble columns and gas-liquid-solid fluidized

- beds.” *AICHE Journal* 50 (2): 288–301.
- Clift, R., J. R. Grace, and M. E. Weber. 1978. *Bubbles, Drops and Particles*. New York: Academic Press.
- Deen, N.G., M. Van Sint Annaland, M.A. Van der Hoef, and J.A.M. Kuipers. 2007. “Review of discrete particle modeling of fluidized beds.” *Chemical Engineering Science* 62 (1-2): 28 – 44.
- Deen, N. G., M. van Sint Annaland, and J.A.M. Kuipers. 2007. “Numerical Simulation of Particle Mixing in Dispersed Gas-Liquid-Solid Flows using a Combined Volume of Fluid and Discrete Particle Approach.” In *6th International Conference on Multiphase Flow, ICMF 2007*, Leipzig. Paper no. 271. <http://doc.utwente.nl/68811/>.
- Deen, N. G., M. van Sint Annaland, and J.A.M. Kuipers. 2009. “Direct numerical simulation of complex multi-fluid flows using a combined front tracking and immersed boundary method.” *Chemical Engineering Science* 64 (9): 2186 – 2201.
- Donath, S., C. Feichtinger, T. Pohl, J. Götz, and U. Rüde. 2009. “Localized Parallel Algorithm for Bubble Coalescence in Free Surface Lattice-Boltzmann Method.” In *Euro-Par 2009 Parallel Processing*, Vol. 5704 of *Lecture Notes in Computer Science* edited by H. Sips, D. Epema, and H.-X. Lin. 735–746. Springer.
- Fan, L.-S., and K. Tsuchiya. 1990. *Bubble Wake Dynamics in Liquids and Liquid-Solid Suspensions*. Boston, London, Singapore, Sydney, Toronto, Wellington: Butterworth-Heinemann.
- Feichtinger, C., S. Donath, H. Köstler, J. Götz, and U. Rüde. 2011. “WaLBerla: HPC software design for computational engineering simulations.” *Journal of Computational Science* 2(2): 105–112.
- Frisch, U., D. d’Humières, B. Hasslacher, P. Lallemand, Y. Pomeau, and J.-P. Rivet. 1987. “Lattice Gas Hydrodynamics in Two and Three Dimensions.” *Complex Systems* 1: 649–707.
- Ginzbourg, I., and P.M. Adler. 1994. “Boundary Flow Condition Analysis for three-dimensional lattice Boltzmann model.” *Journal of Physics II France* 4: 191–214.
- Ginzburg, I., and D. d’Humières. 2009. “Viscosity independent numerical errors for Lattice Boltzmann models: From recurrence equations to ”magic” collision numbers.” *Computers and Mathematics with Applications* 58 (5): 823–840.
- Ginzburg, I., F. Verhaeghe, and D. d’Humières. 2008. “Two-Relaxation-Time Lattice Boltzmann Scheme: About Parametrization, Velocity, Pressure and Mixed Boundary Conditions.” *Communications in Computational Physics* 3 (2): 427–478.
- Götz, J., K. Iglberger, M. Stürmer, and U. Rüde. 2010. “Direct numerical simulation of particulate flows on 294912 processor cores.” In *Proceedings of the 2010 ACM/IEEE International Conference for High Performance Computing, Networking, Storage and Analysis*, 1–11. IEEE Computer Society.
- Grace, J. R. 1973. “Shapes and Velocities of Bubbles Rising in Infinite Liquids.” *Transactions of the Institution of Chemical Engineers* 51: 116–120.
- Harting, J., S. Frijters, M. Ramaioli, M. Robinson, D.E. Wolf, and S. Luding. 2014. “Recent advances in the simulation of particle-laden flows.” *The European Physical Journal Special Topics* 223 (11): 2253–2267.
- Hirt, C. W., and B. D. Nichols. 1981. “Volume of fluid (VOF) method for the dynamics of free boundaries.” *Journal of Computational Physics* 39: 201–225.
- Holdych, D. J., D. R. Noble, J. G. Georgiadis, and R. O. Buckius. 2004. “Truncation error analysis of lattice Boltzmann methods.” *Journal of Computational Physics* 193 (2): 595–619.
- Jansen, F., and J. Harting. 2011. “From bijels to Pickering emulsions: A lattice Boltzmann study.” *Physical Review E* 83: 046707–1 – 046707–11.
- Joshi, A. S., and Y. Sun. 2009. “Multiphase lattice Boltzmann method for particle suspensions.” *Physical Review E* 79: 066703.
- Junk, M., A. Klar, and L.-S. Luo. 2005. “Asymptotic analysis of the lattice Boltzmann equation.” *Journal of Computational Physics* 210: 676–704.
- Körner, C., M. Thies, T. Hofmann, N. Thürey, and U. Rüde. 2005. “Lattice Boltzmann Model for Free Surface Flow for Modeling Foaming.” *Journal of Statistical Physics* 121 (1/2): 179–196.
- Kromkamp, J., D. van den Ende, D. Kandhai, R. van der Sman, and R. Boom. 2006. “Lattice Boltzmann simulation of 2D and 3D non-Brownian suspensions in Couette flow.” *Chemical Engineering Science* 61 (2): 858–873.
- Ladd, A. J. C. 1994. “Numerical simulations of particulate suspensions via a discretized Boltzmann equation. Part 1. Theoretical foundation.” *Journal of Fluid Mechanics* 271: 285–309.
- Ladd, A. J. C., and R. Verberg. 2001. “Lattice-Boltzmann Simulations of Particle-Fluid Suspensions.” *Journal of Statistical Physics* 104: 1191–1251.
- Li, W., and W. Zhong. 2015. “CFD simulation of hydrodynamics of gas-liquid-solid three-phase bubble column.” *Powder Technology* 286: 766 – 788.

- Li, Y., J. Zhang, and L.-S. Fan. 1999. "Numerical simulation of gas-liquid-solid fluidization systems using a combined CFD-VOF-DPM method: bubble wake behavior." *Chemical Engineering Science* 54 (21): 5101–5107.
- Mittal, R., and G. Iaccarino. 2005. "Immersed Boundary Methods." *Annual Review of Fluid Mechanics* 37: 239–261.
- Pan, H., X.-Z. Chen, X.-F. Liang, L.-T. Zhu, and Z.-H. Luo. 2016. "CFD simulations of gas-liquid-solid flow in fluidized bed reactors — A review." *Powder Technology* 299: 235 – 258.
- Panneerselvam, R., S. Savithri, and G.D. Surender. 2009. "CFD simulation of hydrodynamics of gas-liquid-solid fluidised bed reactor." *Chemical Engineering Science* 64 (6): 1119 – 1135.
- Parker, B. J., and D. L. Youngs. 1992. *Two and Three Dimensional Eulerian Simulation of Fluid Flow with Material Interfaces*. Tech. rep.. UK Atomic Weapons Establishment.
- Qian, Y. H., D. d'Humieres, and P. Lallemand. 1992. "Lattice BGK Models for Navier-Stokes Equations." *Europhysics Letters* 17 (6): 479–484.
- Scardovelli, R., and S. Zaleski. 1999. "Direct numerical simulation of free-surface and interfacial flow." *Annual Review of Fluid Mechanics* 31: 567–603.
- Stickel, J. J., and R. L. Powell. 2005. "FLUID MECHANICS AND RHEOLOGY OF DENSE SUSPENSIONS." *Annual Review of Fluid Mechanics* 37: 129–149.
- Stratford, K., R. Adhikari, I. Pagonabarraga, J.-C. Desplat, and M. E. Cates. 2005. "Colloidal Jamming at Interfaces: A Route to Fluid-Bicontinuous Gels." *Science* 309 (5744): 2198–2201.
- Sun, X., and M. Sakai. 2015. "Three-dimensional simulation of gas-solid-liquid flows using the DEM-VOF method." *Chemical Engineering Science* 135: 531–548.
- Tang, Y., E. A. J. F. Peters, J. A. M. Kuipers, S. H. L. Kriebitzsch, and M. A. van der Hoef. 2015. "A new drag correlation from fully resolved simulations of flow past monodisperse static arrays of spheres." *AIChE Journal* 61 (2): 688–698.
- Tenneti, S., R. Garg, and S. Subramaniam. 2011. "Drag law for monodisperse gas-solid systems using particle-resolved direct numerical simulation of flow past fixed assemblies of spheres." *International Journal of Multiphase Flow* 37 (9): 1072–1092.
- Tenneti, S., and S. Subramaniam. 2014. "Particle-Resolved Direct Numerical Simulation for Gas-Solid Flow Model Development." *Annual Review of Fluid Mechanics* 46: 199–230.
- Tryggvason, G., R. Scardovelli, and S. Zaleski. 2011. *Direct Numerical Simulations of Gas-Liquid Multiphase Flows*. Cambridge University Press.
- Tsuchiya, K., A. Furumoto, L.-S. Fan, and J. Zhang. 1997. "Suspension viscosity and bubble rise velocity in liquid-solid fluidized beds." *Chemical Engineering Science* 52 (18): 3053 – 3066.
- van Sint Annaland, M., N.G. Deen, and J.A.M. Kuipers. 2005a. "Numerical simulation of gas bubbles behaviour using a three-dimensional volume of fluid method." *Chemical Engineering Science* 60 (11): 2999 – 3011.
- van Sint Annaland, M., N.G. Deen, and J.A.M. Kuipers. 2005b. "Numerical simulation of gasliquid-solid flows using a combined front tracking and discrete particle method." *Chemical Engineering Science* 60 (22): 6188 – 6198.
- Wolf-Gladrow, D. 2005. *Lattice-Gas Cellular Automata and Lattice Boltzmann Models - An Introduction*. Springer.
- Xu, Y., M. Liu, and C. Tang. 2013. "Three-dimensional CFD-VOF-DPM simulations of effects of low-holdup particles on single-nozzle bubbling behavior in gas-liquid-solid systems." *Chemical Engineering Journal* 222: 292–306.